

Fingerprint, Not Blueprint: How Positional Schemes Set the Default Spectral Algebra of Attention

Li Hengyu¹

¹Institute for Solid State Physics, The University of Tokyo,
lihengyu@issp.u-tokyo.ac.jp

Abstract

The pre-softmax score of an attention head is a bilinear form $\text{score}(i, j) = x_i^\top M x_j$ in a learned operator $M = W_q^\top W_k$. Because M is generally non-symmetric, hence non-normal, it has a complex eigenspectrum and non-orthogonal eigenvectors, the regime where non-Hermitian and random-matrix tools apply. We ask what this spectrum encodes, at three levels for previous-token and induction circuits. Statically, across seven pretrained models spanning three positional schemes, the strongest previous-token heads are spectrally rotational under RoPE and non-rotational, or content-like, where position enters outside QK (learned-absolute and ALiBi); the model-level separation is perfect at every top- k examined (exact permutation $p=0.029$), and zeroing the per-frequency RoPE phase $\text{Im}(M_t)$ eliminates induction on a pre-identified previous-token head in all three RoPE models. Dynamically, over public Pythia checkpoints every head originates at the random-matrix (Ginibre) null; the rotational signature emerges with the behavior, not before it, and the population-median suppression that yields the final profile follows circuit formation, so the profile is a consolidated fingerprint, not a precursor. Causally, and at toy scale, no spectral channel is necessary: constrained two-layer training reroutes around every ban with capability intact, albeit at a significant formation delay (four pre-registered contrasts, $q_{\text{BH}} \leq 0.016$). The cost structure exposes each scheme’s default: imposing symmetry slows learned-absolute models by a factor of 2.9, whereas a RoPE head with a fully symmetric static M still routes directionally via the phase channel, impossible under absolute positions. Within the settings examined, the positional scheme sets the default spectral algebra of an attention head’s solution: a fingerprint sculpted after function, not a hard constraint upon it.

1 Introduction

For a single attention head with norm-processed residual token $x \in \mathbb{R}^d$ and projections W_q, W_k , the pre-softmax score is a bilinear form in one operator,

$$\text{score}(i, j) = q_i^\top k_j = x_i^\top (W_q^\top W_k) x_j = x_i^\top M x_j, \quad M = W_q^\top W_k \in \mathbb{R}^{d \times d}. \quad (1)$$

M is the natural, gauge-invariant object of study: the reparametrization $W_q \rightarrow W_q G$, $W_k \rightarrow W_k G^{-\top}$ leaves M and every observable unchanged, so raw W_q/W_k entries are gauge artifacts while functions of M are physical (6). M is low rank (rank $\leq d_k$) and, crucially, *generally non-symmetric*—so it has a complex eigenspectrum.

A growing literature reads non-normal/complex spectral structure into transformers: Schur decompositions of the residual-stream Jacobian (7), “non-Hermitian” operator-theoretic framings (3), and symmetric/antisymmetric decompositions of the QK matrix (15); concurrent work catalogues per-head complex eigenvalues of the attention interaction and ablates its skew/symmetric channels against corpus perplexity (9). Yet the QK operator’s complex spectrum remains *behaviorally unanchored* — no random-matrix nulls, no head-function taxonomy, no head-resolved causal tests, no positional-scheme contrasts — and the field’s discipline demands we ask not whether the structure *exists* but whether it *does measurable work*. Concretely: does the complex-eigenvalue view of M predict head behavior that the plain symmetric/antisymmetric split does not already capture?

We answer this at three levels: *statics* across seven pretrained models — GPT-2 small, OPT-1.3B, and GPT-Neo-1.3B (learned-absolute positions), BLOOM-1b1 (ALiBi: position enters as a score bias, leaving QK positionally unconstrained), Pythia-410m/1.4B (25% RoPE), and Llama-3-8B (100% RoPE, RMSNorm, GQA); *dynamics* across the public Pythia training checkpoints; and *interventions* in constrained-from-scratch training runs. Our contributions:

1. **A matched-null spectral framework for the QK operator** (§3): four decompositions of the norm-folded M , a primary directionality metric D_{head} and its plain-split baseline `dir_frac`, and—essential—a *random-orientation (Ginibre) null* against which directionality must be read (a random low-rank M already has `dir_frac` $\approx 1/\sqrt{2}$).
2. **Descriptive**: spectral directionality separates head function across all seven models (§4), extending Saponati et al. (15) from training objective to head function.
3. **Causal anatomy** on GPT-2 (§5): the symmetric part M_S is $6.7\times$ more load-bearing than the antisymmetric M_A ; M_A is causally critical only for the canonical induction/previous-token circuit and inert elsewhere. On GPT-2 the complex refinement D_{head} does *not* beat `dir_frac`.
4. **The architecture-conditional signature** (§6): the strongest previous-token heads are spectrally rotational under RoPE (top-quintile D_{head}) and non-rotational under learned-absolute *and* ALiBi positions (bottom-quartile, four models); the model-level separation is perfect at every top- k tested (exact permutation $p=0.029$; head-level $p=2.5\times 10^{-5}$, descriptive); d_k held fixed across schemes. Aggregate partials are shown to be bulk-contaminated and unreliable for this contrast.
5. **Mechanism** (§7): a per-frequency complex decomposition ties D_{head} to the RoPE rotational phase $\text{Im}(M_t)$; adding RoPE-phase features as controls attenuates D_{head} ’s advantage by $\sim 47\text{--}61\%$ (25% RoPE) and $\sim 70\text{--}98\%$ (100% RoPE), estimator-dependent.
6. **Causal confirmation** (§8): ablating $\text{Im}(M_t)$ symmetrizes the relative-position kernel and destroys induction on exactly the flagged heads.
7. **A checkpoint natural history** (§9): on Pythia-410m/160m (22 public checkpoints each), all heads are born at the Ginibre null; the rotational signature locks in *with* circuit formation (not before it), and the population-median suppression that produces the static profile follows formation — the profile is a consolidated fingerprint, not a precursor.
8. **Constrained-training interventions** (§10): a $\{\text{APE, RoPE}\} \times \{\text{free, sym-}M, \text{Im}(M_t)\text{-suppressed}\}$ grid ($n=5$ seeds) shows no spectral channel is *necessary* (every arm reroutes) while every constraint carries a significant search cost that reveals the scheme’s default solution, and dissociates the static-antisymmetry and RoPE-phase channels at the weight level.

One sentence unifies the three levels: *the positional scheme sets the default spectral algebra of attention’s solutions — a fingerprint sculpted after function, an economy of search rather than a*

hard constraint. We report the negatives (GPT-2 decorativeness; M_A ’s inertness away from a few heads) as plainly as the positives.

2 Related work

QK circuits and weight-space interpretability. Elhage et al. (6) frame $M=W_q^\top W_k$ and W_{OV} as the two low-rank circuits and use OV eigenvalue positivity as a copying statistic; they perform no QK spectral analysis. Millidge and Black (12) find weight-SVD interpretable but report it *fails* on QK—motivating an orientation-recovering (Schur/complex) view. Our object and the OV/QK distinction follow this line; our contribution is the QK-side, imaginary-axis, behavior-anchored analog.

Symmetric/antisymmetric QK. Saponati et al. (15) decompose $W_{qk}=M_s+M_n$ and define a Frobenius symmetry score, anchoring it to the *training objective*. Our `dir_frac` is a monotone transform of their score ($s = 1 - 2 \text{dir_frac}^2$); we anchor the split to *head function* and add the complex/Schur refinement and its causal test.

Non-normal / non-Hermitian transformers. Concurrently with this work, Jamil and Kapadia (9) decompose the per-head attention interaction into skew (“routing”) and symmetric (“filtering”) channels across 1,776 heads of five pretrained models, report $\max \text{Re } \lambda > 0$ for every head, find by all-heads truncation surgery on GPT-2 Large that the symmetric channel is by far the more load-bearing (convergent, at the aggregate level, with our §5), and train a stability-constrained skew-minus-diagonal attention from scratch. Their analysis stops at norms, ranks, and stability — no behavioral taxonomy, no random-matrix null, no head-resolved causal test, no positional-scheme contrast, and their weight-level routing–filtering ratio is (like Saponati’s score) a monotone transform of `dir_frac`— so it cannot ask whether the complex spectrum does work *beyond* the plain split; that anchoring is our contribution. Fernando and Guitchounts (7) Schur-decompose the residual-stream *Jacobian* and show learned non-normality is functionally central—but on a different operator, without pseudospectra, and anchored to rank/propagation, not head function. Chang (3) labels $W_q^\top W_k$ non-Hermitian in a Dyson-series theory with no computation. We differ by analyzing the QK operator’s complex spectrum empirically and anchoring it to head behavior.

RoPE and positional heads. RoPE (17) injects $e^{im\theta_t}$ phase, $\theta_t = \text{base}^{-2t/d}$. Barbero et al. (1) and Urrutia et al. (19) show positional heads use high RoPE frequencies. We connect a *weight-space* directionality scalar to per-head RoPE-frequency usage and to head function, which they do not.

Circuit formation over training. Olsson et al. (13) established the induction phase change; Tigges et al. (18) track circuits across all Pythia checkpoints behaviorally (induction at $\sim 2 \times 10^9$ tokens); toy-model studies dissect formation (2, 14, 16); and Chen et al. (4) regularize an interpretable attention property during MLM pretraining — the template our intervention ports to autoregressive weight space. Saponati et al. (15) track their symmetry score during training (per-layer, own encoder/decoder runs). None of these tracks a weight-space spectral quantity per head across public checkpoints against the phase change (§9), and none constrains QK spectral structure during autoregressive training (§10).

Constrained-attention training. Hard symmetric (shared-QK) causal LMs exist — Reformer (10) and recent systematic sharing studies — and symmetric dot-product BERT trains well (5), but none analyzes circuits under the constraint, and the soft, decomposed versions (penalize only M_A , or only $\text{Im}(M_t)$) are new here; concurrent observational work crosses positional schemes with induction formation in toy models (8).

Head taxonomy. We use standard detectors—previous-token, duplicate, induction (13)—and

IOI (20) head classes for validation.

3 Method

Object and folding. We use TransformerLens with `fold_ln=True` to absorb the norm gain into W_q, W_k , and analyze the norm-folded operator $M_{\text{eff}} = CMC$ for LayerNorm (centering $C = I - \frac{1}{d}\mathbf{1}\mathbf{1}^\top$) and $M_{\text{eff}} = M$ for RMSNorm. All spectral work is float64. We verify the convention by reconstructing the model’s own pre-softmax scores from M and matching to $< 10^{-4}$ (learned-absolute) or, for RoPE models where position cancels only at $i=j$, matching the diagonal (bf16 models match to bf16 precision; the fast metric path is exact, `dir_frac` $\Delta=10^{-16}$). A random $G \in GL(d_k)$ leaves M , its eigenvalues, and D_{head} invariant to $\sim 10^{-14}$ while changing raw column norms—confirming gauge hygiene.

Decompositions. Per head we compute the SVD, the symmetric/antisymmetric split $M=M_S+M_A$, the real Schur form (2×2 blocks \rightarrow rotation angles θ), and the complex eigen-decomposition (with eigenvector condition number as a non-normality flag).

Metrics.

$$\text{dir_frac} = \|M_A\|_F / \|M\|_F \quad (\text{plain antisymmetric magnitude; Saponati’s score}) \tag{2}$$

$$D_{\text{head}} = \sum_r |\text{Im } \lambda_r| / \sum_r |\lambda_r| \quad (\text{primary complex/Schur directionality}) \tag{3}$$

$$\text{content_pos_frac} = \sum \lambda^+ / \sum |\lambda| \text{ of } M_S \quad (\text{signed content axis; QK-side echo of OV positivity}) \tag{4}$$

plus `henrici` = $\sqrt{\|M\|_F^2 - \sum |\lambda|^2} / \|M\|_F$ (departure from normality) and `self_match` (diagonal dominance of $W_E M W_E^\top$).

The random-orientation null (essential). A random low-rank M is already highly “directional”: for independent Gaussian W_q, W_k the symmetric and antisymmetric parts get equal expected Frobenius mass, so `dir_frac`_{null} $\approx 1/\sqrt{2} \approx 0.707$ and D_{head} ’s null is likewise high. We therefore report every metric relative to a *matched- Σ random-orientation null* (same singular values, random left/right frames), computed exactly in the rank- k core. Empirically `dir_frac`_{null}=0.707, $D_{\text{head},\text{null}}$ =0.608; 141/144 GPT-2 heads deviate ($|z|>2$ on `dir_frac` or D_{head} ; `dir_frac` alone: 140/144). Nulls are computed exhaustively for GPT-2; the cross-model analyses of §6 use raw metrics — on GPT-2, null-referenced metrics give an indistinguishable partial (-0.204 vs -0.206), so this choice is not load-bearing.

Models & corpus. GPT-2 small (144 heads), OPT-1.3B (768), GPT-Neo-1.3B (384), BLOOM-1b1 (384; ALiBi), Pythia-410m/1.4B (384), Llama-3-8B (1024; GQA expanded, RMSNorm, bf16). Behavioral runs use a $1k \times 128$ slice of NeelNanda/pile-10k; detectors use repeated-random sequences. All on one A100.

Checkpoint and intervention pipelines. For §9 we load Pythia public checkpoints natively (TransformerLens `checkpoint_value`); the fused-QKV unpacking and folding conventions were verified against the main-revision pipeline to machine precision (weight metrics at the final checkpoint match the independent pipeline exactly, $\Delta=0$). For §10 we train 2-layer attention-only models from scratch with soft spectral penalties; definitions and the crucial $\text{sym-}M \neq \text{Im}(M_t)$ distinction are given there. Pre-registration: the dynamics questions (Q1–Q3) and intervention predictions (P1–P4) were locked in the project’s intervention plan before any checkpoint was downloaded or any constrained run launched; we report the falsified predictions as findings.

metric	prev-token	duplicate	induction	copying (OV)
<code>dir_frac</code>	+0.47	-0.59	-0.50	0.06 (ns)
<code>content_pos_frac</code>	-0.63	+0.59	+0.57	ns
<code>imag_mass</code>	+0.56	-0.65	-0.61	ns

Table 1: Spearman correlations of spectral metrics with head-type scores (GPT-2, $n=144$; all shown are FDR-significant). Copying is an orthogonal OV-side control.

4 Spectral directionality separates head function

On GPT-2 ($n=144$, Spearman, BH-FDR $q < 10^{-3}$), directionality maps onto head class (Table 1). Previous-token heads are directional (high `dir_frac`, low content positivity); duplicate/similarity heads are symmetric; **induction heads read as content-like**. We note plainly that our pre-registered hypothesis predicted the opposite (induction heads directional); that prediction *failed*. The two-head-circuit reading — the induction head’s QK consumes *composed content* written by a previous-token head, so its single-head M is symmetric — was recorded in the analysis plan before these correlations were computed, and we verify it directly: by the K-composition statistic (the Frobenius overlap of an induction head’s QK operator with an earlier head’s OV write, ranked over all earlier heads), **the canonical previous-token head ranks #1 for every induction head tested** — GPT-2’s 4.11 for 5.1/5.5/6.9 (ranks 1/60, 1/60, 1/72) and Pythia-410m’s 5.2 for 8.6/10.9/11.14 (1/128, 1/160, 1/176) — confirming that induction QK is wired to consume the prev head’s composed output. **Copying (OV) is orthogonal to every QK metric**, a clean control. The content signature is legible: `self_match` equals `content_pos_frac` at $r=0.96$; empirical pre-softmax score asymmetry on real inputs tracks `dir_frac` at 0.66. This replicates on Pythia and, attenuated, on Llama (`content_pos_frac` \rightarrow prev -0.30 vs GPT-2’s -0.63 ; §6), establishing spectral directionality as an architecture-general head-function signature and extending Saponati et al. (15) from objective to function (Fig. 1).

5 Causal anatomy on GPT-2: $M_S \gg M_A$

Symmetrization ablation. Replacing a head’s M with M_S (killing M_A) or M_A (killing M_S) and measuring held-out CE, the **symmetric part is $6.7\times$ more load-bearing**: $\sum \Delta CE_{\text{anti}}=2.60$ vs $\sum \Delta CE_{\text{sym}}=0.39$; killing M_A costs ≤ 0.02 general CE anywhere. But a *targeted induction task* exposes that M_A is causally *essential* for specific heads: killing it on the canonical induction head 5.1 raises induction loss $8\times$ ($0.21 \rightarrow 1.77$; $15\times$ the next-largest effect) and on the previous-token head 4.11 by $\sim 50\%$. Canonical induction heads 5.5/6.9 show smaller positive effects ($+0.03$, ranks 7–8 of 144); the top-5 by effect are 5.1, 4.11, 6.7, 3.0, 8.5, so top-5 overlap with the canonical circuit is $2/5$ (hypergeometric $p=0.014$), with the argmax landing on a canonical induction head — circuit-level enrichment, not an exact circuit match. Crucially this importance is a **discrete circuit fact**: no spectral scalar (`dir_frac`, D_{head} , `imag_mass`, $\|M_A\|$) predicts *which* heads need M_A (all $|\rho| \lesssim 0.1$), so the 144-head aggregate is null.

Incremental validity. For predicting the previous-token score, the complex refinement adds no reliable positive increment on GPT-2: $\text{partial } \rho(D_{\text{head, prev}} \mid \text{dir_frac}) = -0.21$ (layer-clustered 95% CI $[-0.51, +0.08]$ — the point estimate is negative but not reliably so; among prev-candidate heads, $\text{prev} > 0.05$, the residual association is strongly negative, -0.63), and in a nested regression on the ablation effect `dir_frac` explains 0.001 of variance rising only to 0.028 with D_{head} added, the added term wrong-signed. On learned-absolute positions, the plain antisymmetric magnitude

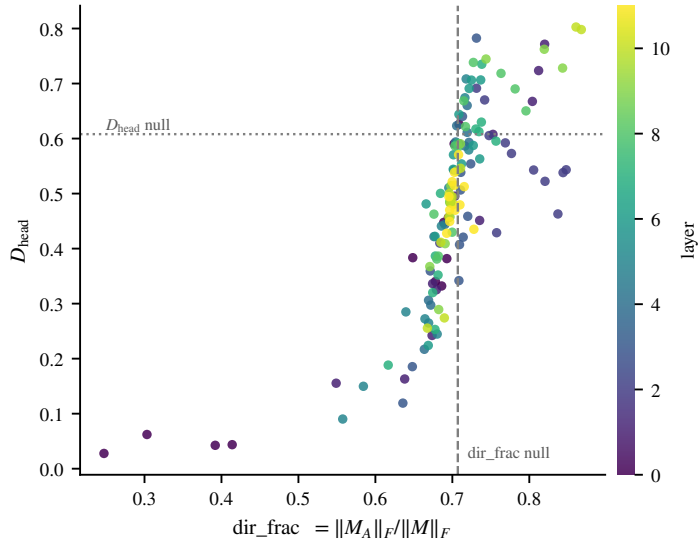


Figure 1: The content–direction plane (GPT-2). Each point is a head; dashed lines mark the random-orientation null ($\text{dir_frac}_{\text{null}} \approx 0.707$, $D_{\text{head}, \text{null}} \approx 0.608$). A content cluster (low on both, mostly layer 0) sits below the null; directionality is read as deviation from it.

captures everything the complex spectrum reliably offers about its strong prev heads; §6 shows this head-profile pattern generalizes to OPT-1.3B and GPT-Neo-1.3B, though their aggregate statistics do not.

6 The architecture-conditional signature (main result)

We run the incremental-validity test across positional schemes on seven models (Table 2). On every RoPE model, D_{head} ’s incremental contribution beyond dir_frac is positive and robust (clustered CIs [+0.21, +0.59]). Under learned-absolute positions, however, the *aggregate* statistic is heterogeneous (GPT-2 −0.21; OPT-1.3B +0.35; GPT-Neo-1.3B +0.20) — and decomposing it shows why it is the wrong statistic: a positive gradation among near-zero-prev *bulk* heads is present in most models (including GPT-2: +0.25 within $\text{prev} \leq 0.05$), while the signal that differs by architecture lives in the *strong* previous-token heads themselves. The last column of Table 2 gives each model’s top-5 prev heads’ within-model D_{head} percentile: **bottom-quartile under learned absolute** (medians 0.21/0.23/0.14; e.g. GPT-2’s 4.11 at 0.22; all with content-like symmetric profiles, content_pos_frac 0.46–0.57) and ALiBi (0.26) versus **top-quintile under RoPE** (medians 0.89/0.85/0.79; Fig. 2a). Holding $d_k=64$ fixed (GPT-2, OPT-1.3B, Pythia-410m: 0.21/0.23 vs 0.89) ties the contrast to the positional scheme, not head dimension.

Model-level inference and sensitivity. Heads within a model share training, layers, and detectors, so the model is the honest experimental unit. At model level the separation is *perfect* — every non-RoPE model’s top-5 median sits below every RoPE model’s — giving an exact model-level permutation $p=1/\binom{7}{3}=0.029$, the minimum attainable with seven models; the head-level joint Mann–Whitney $p=2.5 \times 10^{-5}$ is reported as descriptive only. The contrast is not an artifact of the $k=5$ choice: model-level separation is perfect at every $k \in \{1, 3, 5, 10\}$, and leave-one-model-out preserves it for all seven models. The binding statistical limit is the model count itself — one ALiBi and one full-RoPE family — which more model families, not more heads, would address

(Limitations). The defensible claim is *profile-level*: **the heads that implement previous-token attention are spectrally rotational under RoPE and spectrally non-rotational (content-like) under learned absolute positions**. Mechanistically, this is what the positional algebra dictates: with learned absolute embeddings, prev-token attention can be built by *matching* adjacent position vectors — a symmetric, content-like operation — whereas RoPE builds it from *rotations*, imprinting complex eigenstructure. **ALiBi provides the cleanest test**: position enters as a score *bias*, so QK needs no positional structure at all — and BLOOM-1b1’s top prev heads are indeed non-rotational (percentile 0.26), patterning with the learned-absolute group exactly as the mechanism predicts. Under RoPE these heads sit at the `dir_frac` null (~ 0.70) with D_{head} at the Ginibre value (≈ 0.61) while the population suppresses below it (medians 0.40–0.45; per-model matched nulls: 410m prev heads’ $D_{\text{head}} z \in [-0.1, +5.0]$ vs population median $z = -11$; 1.4B prev-head median $z = -3.7$ vs population $z = -13.9$): they *retain* near-random rotational structure that other heads learn to suppress, and the Schur/complex view detects this where the Frobenius magnitude cannot.

Robustness and scope. Three qualifications sharpen the claim. (i) *Metric specificity*: among complex-spectrum summaries, `imag_mass` is incrementally positive on all models and Henrici non-normality negative on all; D_{head} composites these two channels. No single aggregate scalar separates the schemes — the head-profile statistic does. (ii) *Class vs bulk*: the RoPE positives are class-level separation (rank-biserial +0.44/ +0.60 at `prev>0.2` in Pythia; +0.29 at `prev>0.1` in Llama) *plus* bulk gradation; within confirmed prev heads there is no further gradation (subset partials n.s.). Under learned-absolute positions the class-level tests are null-to-negative at the strong end (GPT-2 -0.39 at `prev>0.2`, significant; OPT -0.11 n.s.; GPT-Neo +0.13 n.s.), though GPT-Neo shows a positive signal at the looser `prev>0.1` band (+0.34) driven by its moderate-prev heads — its *top* prev heads still sit at percentile 0.14. The learned-absolute models are thus heterogeneous in their moderate bands (candidate sources: training corpus, GPT-Neo’s alternating local-attention layers) while uniform at the top of the class. (iii) GPT-2’s negative aggregate concentrates exactly among prev-candidate heads (-0.63 at `prev>0.05`); OPT’s positive aggregate is entirely bulk (-0.18 among its prev candidates). Aggregate partials should not be read as the architecture signal in either direction.

7 Mechanism: D_{head} tracks the RoPE phase

RoPE pairs each head’s d_k dims (rotate-half convention, verified) into frequencies θ_t ; the QK interaction per frequency is a rank-1 complex sub-operator $M_t = w_q^t \overline{w_k^t}^\top$, with the static $M = \sum_t \text{Re}(M_t)$. The *directional* (relative-position-asymmetric) content is carried by the imaginary part:

$$\text{score}(\Delta) - \text{score}(-\Delta) = \sum_t 2 \sin(\Delta\theta_t) n^\top \text{Im}(M_t) n. \tag{5}$$

(Full-score reconstruction from $\{M_t, \theta_t\}$ matches the model to $10^{-6}/10^{-2}$ in fp32/bf16.) Empirically, previous-token heads have high rotary directional fraction `rope_imag_frac` (correlation with `prev`: +0.53/ +0.42/ +0.50 for 410m/1.4B/Llama) concentrated at *high frequencies* (+0.68 on full-RoPE Llama—a Barbero et al. (1), Urrutia et al. (19) replication), and D_{head} **tracks this deployment**. Adding per-frequency RoPE-phase summaries as controls *attenuates* D_{head} ’s residual association substantially (Table 3) — most completely on full-RoPE Llama, where the default-estimator residual is indistinguishable from zero (+0.006, $p=0.84$; fully rank-based: +0.075, $p=0.016$). Two qualifications. First, all quantities are co-derived from the same weights, so this is shared-variance accounting, not causal mediation. Second, the attenuating covariate *changes identity* with RoPE

model	d_k	positions	norm	ρ_{dir}	ρ_D	partial	95% CI	top-5 pctile
GPT-2	64	absolute	LN	+0.47	+0.29	-0.21	[-0.51, +0.08]	0.21
OPT-1.3B	64	absolute	LN	+0.08	+0.28	+0.35	[+0.19, +0.48]	0.23
GPT-Neo-1.3B	128	absolute	LN	+0.35	+0.41	+0.20	[+0.07, +0.33]	0.14
BLOOM-1b1	96	ALiBi	LN	+0.13	+0.25	+0.34	[+0.22, +0.47]	0.26
Pythia-410m	64	RoPE 25%	LN	+0.57	+0.62	+0.35	[+0.21, +0.47]	0.89
Pythia-1.4B	128	RoPE 25%	LN	+0.31	+0.60	+0.50	[+0.38, +0.59]	0.85
Llama-3-8B	128	RoPE 100%	RMS	+0.32	+0.38	+0.33	[+0.21, +0.45]	0.79

Table 2: Incremental validity of D_{head} over `dir_frac` for the previous-token score, seven models / three positional schemes. $\rho_{\text{dir}} = \rho(\text{dir_frac}, \text{prev})$, $\rho_D = \rho(D_{\text{head}}, \text{prev})$; partial = partial $\rho(D_{\text{head}}, \text{prev} \mid \text{dir_frac})$ (Spearman of OLS residuals); CIs: layer-clustered bootstrap (heads share layers/training, design effects 3.6–6.9; Llama heads additionally share K-projections within GQA groups of 4). **The aggregate partial is heterogeneous under learned-absolute positions** ($-0.21/+0.35/+0.20$) because it mixes a near-ubiquitous positive bulk gradient (among near-zero-prev heads) with the class-level signal; **the architecture-conditional statistic is the last column** — the median within-model D_{head} percentile of the top-5 previous-token heads: bottom-quartile under learned-absolute and ALiBi vs top-quintile under RoPE (perfect model-level separation, exact permutation $p=0.029$; head-level $p=2.5 \times 10^{-5}$, descriptive). $d_k=64$ is shared by GPT-2, OPT-1.3B, and Pythia-410m, so the contrast tracks the positional scheme, not head dimension. All RoPE partials survive BH-FDR.

fraction: on partial-RoPE Pythia the attenuation runs through `rope_imag_frac` (how *much* rotary content is directional; `freq_centroid` alone attenuates nothing, +0.35), whereas on full-RoPE Llama it runs almost entirely through `freq_centroid` (*where in frequency* the directional mass sits: alone +0.33 \rightarrow -0.00, while `rope_imag_frac` alone leaves +0.32) — consistent with all directional content being rotary by construction at 100%, shifting the informative axis from amount to location. The pattern is consistent with fuller attenuation at higher RoPE fraction, but with two dose levels and within-dose spread (61% vs 38%) comparable to the dose gap, we do not press a dose–response reading. The relative-position kernel confirms these heads peak at $\Delta=-1$ with RoPE-periodic oscillation (Fig. 3, left).

Placebo controls. Two controls calibrate what the attenuation means. (i) *RoPE-model specificity*: on all three learned-absolute models (no RoPE), computing a pseudo-`rope_imag_frac` with a fake rotate-half pairing over all head dims yields no prev signal (GPT-2 -0.14, OPT-1.3B -0.06, GPT-Neo-1.3B -0.09; all n.s., vs +0.42–+0.53 on RoPE models), and adding the pseudo-phase features barely attenuates (4–22%): the recipe finds nothing where RoPE is absent. (ii) *Pairing specificity*: randomly permuting the rotary columns of W_Q, W_K — which leaves M (hence $D_{\text{head}}, \text{dir_frac}$) unchanged and preserves rotary-*block* membership, but scrambles the pairing and frequency assignment — still attenuates 31–38% on average, so much of the attenuation is carried by rotary-block membership alone. The increment specific to the *true* pairing/frequency assignment is marginal on Pythia-410m (true 60.7% vs the permutation null, empirical $p=0.039$, $n=50$ permutations) and not significant on Pythia-1.4B (37.7%, $p=0.12$). The mechanism is thus RoPE-specific and largely block-level; the finer pairing-level reading should be held lightly.

8 Causal confirmation: ablating $\text{Im}(M_t)$

We ablate a head’s directional RoPE content by zeroing $\text{Im}(M_t)$ (dropping the $\sin(\Delta\theta)$ component), which **symmetrizes** its relative-position kernel; the decomposition full = symmetric + directional

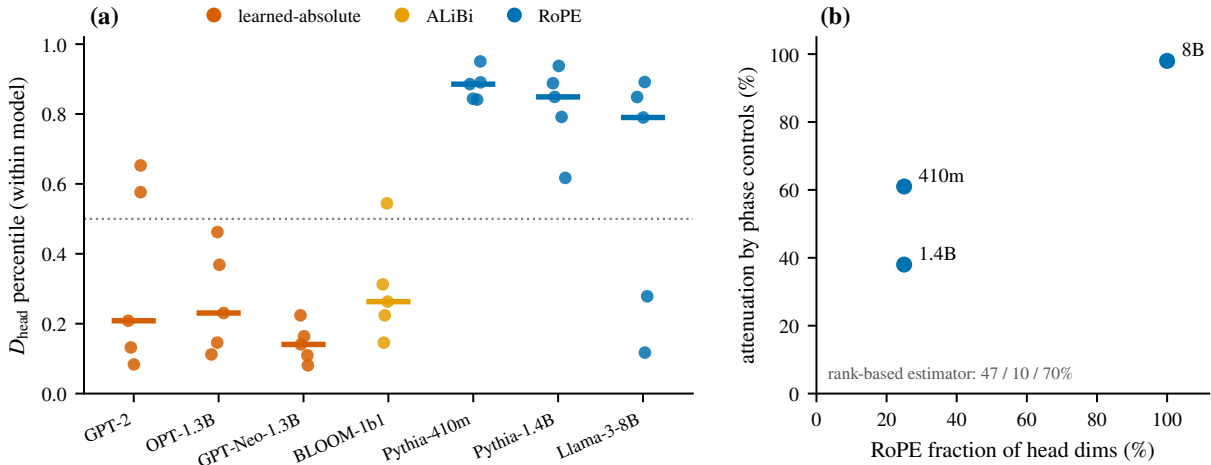


Figure 2: **(a)** Within-model D_{head} percentile of each model’s top-5 previous-token heads: bottom-quartile under learned-absolute (red) and ALiBi (orange) positions, top-quintile under RoPE (blue); joint Mann–Whitney $p=2.5\times 10^{-5}$; bars mark per-model medians. **(b)** Attenuation of D_{head} ’s advantage by RoPE-phase controls grows with RoPE fraction (hybrid estimator: 61%/38% at 25%, $\sim 98\%$ at 100%; see Table 3 for estimator sensitivity — with two dose levels this is suggestive, not an established dose–response).

model	RoPE frac.	partial	+phase controls	atten. (hybrid)	atten. (rank)
Pythia-410m	25%	+0.35	+0.14	61%	47%
Pythia-1.4B	25%	+0.50	+0.31	38%	10%
Llama-3-8B	100%	+0.33	+0.006 ($p=0.84$)	$\sim 98\%$	70%

Table 3: Attenuation of D_{head} ’s residual prev-token association (partial = partial $\rho(D_{\text{head}}, \text{prev} \mid \text{dir_frac})$) when per-frequency RoPE-phase summaries (`rope_imag_frac`, `freq_centroid`) are added as controls. “Hybrid” is the paper’s default estimator (Spearman of OLS residuals); “rank” is fully rank-based, under which the Llama residual is small but nonzero ($+0.075$, $p=0.016$). All quantities are deterministic functions of the same weights: this is shared-variance accounting among co-derived features, *not* causal mediation.

is verified to 6×10^{-6} (fp32; 2×10^{-5} on bf16 Llama). Sweeping the ablation over *all* heads of all three RoPE models, the largest induction-loss effect lands **on a top-2 prev-scoring head every time** — an identity predicted a priori: Pythia-410m head 5.2 (prev rank 1/384; prev 0.95, D_{head} 0.61): induction CE $0.52 \rightarrow 2.24$ ($\sim 4\times$; exact permutation $p=1/384$); Pythia-1.4B head 1.11 (rank 1/384): $0.56 \rightarrow 1.11$ ($\sim 2\times$; $p=1/384$); Llama-3-8B head L14.H26 (rank 2/1024; prev 0.65, D_{head} 0.61): $0.30 \rightarrow 0.91$ ($\sim 3\times$; $p=2/1024$) — jointly $\approx 10^{-8}$ under random assignment. (Llama’s #1 prev head sits in layer 0, too early to feed induction; the causally-critical head is the mid-depth prev head.) Effects are highly concentrated: 92–99% of heads move by $|\Delta \text{Ind}| < 0.01$; the *other* $\text{prev} > 0.5$ heads show ≈ 0 effects (consistent with redundancy across a multi-head circuit), and a few low-prev heads show small effects (≤ 0.17), suggesting downstream circuit participation the prev detector does not capture; head-level aggregate correlations are correspondingly null. The before/after kernel shows the $\Delta = -1$ peak flattening (Fig. 3, right). As in §5, causal importance is concentrated, not a smooth spectral gradient; what the ablation establishes is an *existence-with-*

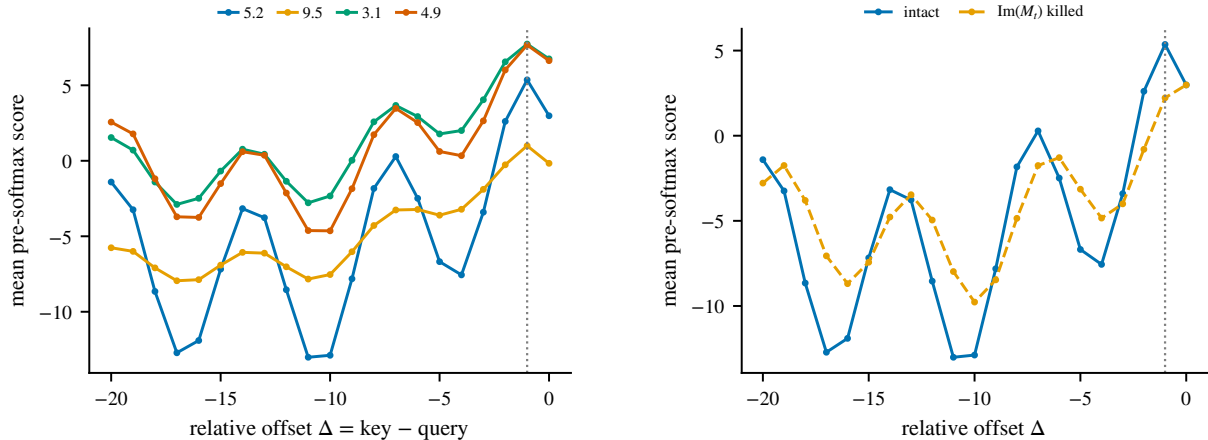


Figure 3: **Left:** corpus-averaged relative-position score kernels of top previous-token heads (Pythia-410m) peak at $\Delta=-1$ with RoPE-periodic oscillation. **Right:** ablating $\text{Im}(M_t)$ on the induction-feeding head 5.2 flattens the $\Delta=-1$ peak (and raises induction loss $4\times$).

predicted-identity claim: the rotational phase D_{head} reads is causally load-bearing for positional routing in the specific heads that carry it.

9 When the imprint arises: a checkpoint natural history

The static profile (§6) is an end-state. To see how it arises we track 22 public checkpoints each of Pythia-410m and Pythia-160m (log-spaced steps $0 \dots 143,000$; the dense early grid straddles the induction onset at $\sim 2 \times 10^9$ tokens (18)), measuring per head: the audited weight metrics (`dir_frac`, D_{head} , `rope_imag_frac`), behavioral previous-token and prefix-matching scores, an in-context-learning proxy (second-copy minus first-copy NLL on repeated-random sequences), and the K-composition wiring between each model’s eventual prev head and its induction heads. (The “eventual prev head” is identified retrospectively at the final checkpoint; Q3 below tests — and rejects — its prospective identifiability.)

A three-act history at half-doubling checkpoint resolution, replicated across both models (Fig. 4). *Act I (0–0.5B tokens): silence at the null.* Every head sits at the Ginibre null (behavior 0.01; `rope_imag_frac` 0.500; population median D_{head} 0.61; K-composition at baseline) — step 0 doubles as an in-vivo verification of the paper’s random-orientation null. *Act II (1–4B tokens): sharp formation.* Previous-token behavior jumps first (0.37 at step 512 \rightarrow 0.95 at step 1000 — the same steps, and even the same 0.37 waypoint, in both models), with induction behavior, the ICL proxy, and the K-composition wiring following within the same window. The prev head’s *within-model rotary-phase* (`rope_imag_frac`) *percentile* snaps from at-or-below chance (0.03–0.04 at step 512, mid-formation, in both models) to the top decile (0.90–0.99) by step 1000: the signature locks in *with* the behavior — at our half-doubling resolution, neither leads. *Act III (4–300B tokens): slow differential sculpting.* The population median D_{head} is suppressed well below the null (0.61 \rightarrow 0.395 / 0.453) over the next $100\times$ of training while the previous-token heads retain it, and the absolute rotary-phase content of the prev head consolidates slowly (0.500 \rightarrow 0.578, same endpoint in both models). The static “retain-vs-suppress” profile of §6 is therefore the end state of a post-formation differentiation process.

Pre-registered answers. Q1 (lead/lag): the percentile signature is *simultaneous* with for-

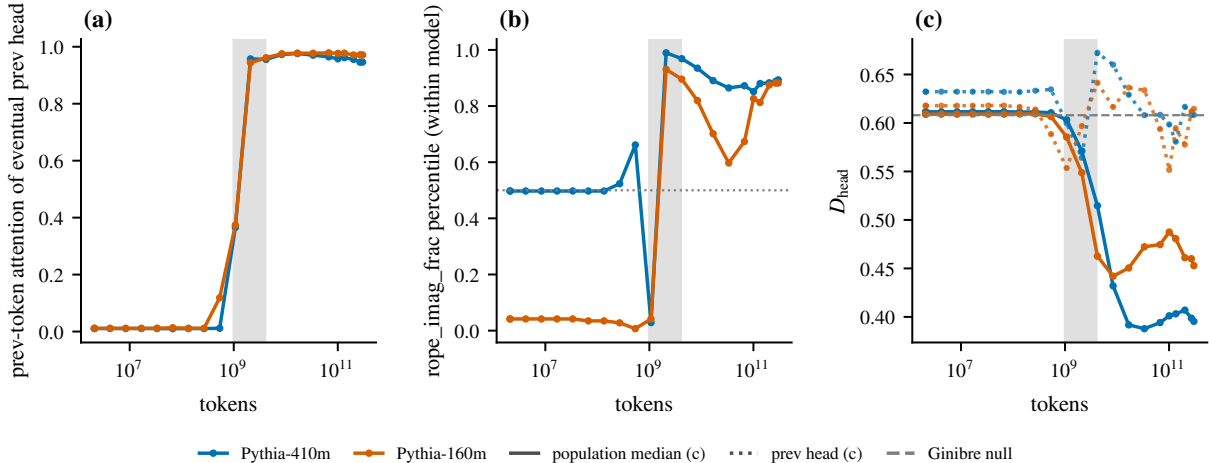


Figure 4: Checkpoint natural history, Pythia-410m (blue) and 160m (red); grey band = the formation window ($1\text{--}4 \times 10^9$ tokens). (a) previous-token behavior forms sharply and identically in both models. (b) the prev head’s `rope_imag_frac` percentile locks in *with* behavior, not before. (c) the population median D_{head} is suppressed below the Ginibre null only *after* formation.

mation; the absolute consolidation *lags*. Q2: population suppression is a post-formation process. Q3 (predictive signature): **no** — before formation the eventual prev head is not reliably identifiable from its spectrum (its percentile even sits low mid-formation); we report this pre-registered negative plainly. The natural history thus bounds what statics can claim: the rotational imprint is the fingerprint the algorithm leaves in weight space, consolidated after function — and because observation cannot order structure and function within the formation window, necessity can only be settled by intervention.

10 Is the rotational channel necessary? Constrained-training interventions

We train 2-layer attention-only models ($d=128$, 4 heads, $d_k=32$) from scratch on a per-sequence random-map task — $x_{t+1} = f_{\text{seq}}(x_t)$ w.p. 0.9, uniform noise w.p. 0.1, with f_{seq} resampled every sequence — which forces induction (no global memorization; no fixed-offset shortcut) and yields a crisp formation time. Grid: {APE, RoPE} \times {free; sym- M : penalize $\|M_A\|_F^2 / \|M\|_F^2$; Im(M_t)-suppressed (RoPE only): penalize $\sum_t \|\text{Im}(M_t)\|_F^2 / \sum_t (\|\text{Re}\|^2 + \|\text{Im}\|^2)$, $n=5$ seeds. A load-bearing algebraic point shapes the grid: **symmetrizing the static M does not zero Im(M_t)** (the static operator contains only the Re parts, $M = \sum_t \text{Re}(M_t) + M_{\text{non-rot}}$), so the two constraints dissociate the static-antisymmetry and phase channels. Both penalties enforce hard (final Im share 0.000; `dir_frac` 0.004–0.006) and no arm loses final capability (all reach the task floor with strong prev and induction heads).

Results against the pre-registered predictions (Fig. 5; Table 4). P1 (free base rates) holds: APE forms fastest (600 ± 0 steps), RoPE free at 940 ± 55 . P2’s strong form is **falsified**: suppressing the phase to zero delays formation only $\sim 1.4\times$ and the circuit *reroutes* — the prev head re-forms with `rope_imag_frac`=0.005 and a qualitatively different (cos-only) relative-position kernel whose peak still lands at $\Delta=-1$. P3 is **falsified in the opposite direction, our largest surprise**: forcing symmetry on APE is the *costliest* constraint in the grid ($600 \rightarrow 1740 \pm 241$, $2.9\times$) — the fast APE

pre-registered contrast (formation delay)	MWU exact p	q_{BH}	rank-biserial	HL shift
P1 RoPE free > APE free	0.0040	0.016	+1.00	+300 steps
P3 APE sym- M > APE free	0.0040	0.008	+1.00	+ 1200 steps (2.9 \times)
P4 RoPE sym- M > RoPE free	0.0040	0.005	+1.00	+600 steps
P2 RoPE Im-sup > RoPE free	0.0079	0.008	+0.92	+400 steps

Table 4: Constrained-training formation delays ($n=5$ seeds per cell; one-sided exact Mann–Whitney, BH-FDR over the four pre-registered contrasts). Every constraint delays formation significantly; none blocks it.

solution is *antisymmetric* embedding-matching, and the symmetric variant (nearby-kernel + causal mask), while reachable, is much harder to find; trained learned-absolute LLMs end at symmetric profiles (§6) with 1000 \times more data, and the toy exposes the search cost of that end state. P4’s formation-time version fails (RoPE+sym delays 1.66 \times) but its **mechanistic dissociation lands exactly**: the sym-arm’s prev head carries *full* phase content (`rope_imag_frac` 0.52) through a *fully symmetric* static operator (`dir_frac` 0.004–0.005), and its positional kernel is indistinguishable from the free arm’s — directional attention through a symmetric M , which is impossible under absolute positions.

Verdict. No spectral channel is *necessary* — the solution space is degenerate and training reroutes around every constraint we imposed — but each constraint carries a significant, quantifiable search cost (Table 4), and the cost structure identifies each scheme’s *default* solution. With §5 and §8 this completes a three-way distinction the field often conflates: *trained-circuit dependence* (post-hoc ablations are catastrophic), *developmental preference* (defaults are found much faster), and *necessity* (nothing here is strictly necessary). A companion note (11) tests the constructive converse — ban-free *assistance* — and finds it selects the same implementations far more cheaply than banning them (1.3 \times vs. 2.9 \times for the antisymmetric-to-symmetric flip) while solution-specific initialization accelerates formation outright, evidence that this spectral economy is not only priced but steerable.

11 Discussion

What earns its keep, and where. The plain symmetric/antisymmetric split of M is an architecture-general descriptor of head function (§4) and, causally, the symmetric part is the workhorse (§5). The *complex-eigenvalue refinement* is architecture-conditional at head level: the previous-token solution is spectrally non-rotational (content-like) under learned-absolute positions and rotational under RoPE, where D_{head} tracks the rotational phase whose causal load §8 establishes head-locally (§6–8). This gives the recent “non-Hermitian transformer” program a concrete, controlled home—the complex structure of the QK operator does measurable, causal work precisely when position is encoded as complex phase—while honestly bounding it: on GPT-2 the non-Hermitian label is decorative.

Practical reading. For weight-only head triage: under RoPE, `rope_imag_frac` (or the D_{head} percentile) flags positional-routing heads without a forward pass; under absolute/ALiBi schemes the same statistics are *misleading in aggregate* (bulk gradients) and only the strong-head profile is informative. For interpretability methodology, the dynamics result is a caution: a clean static weight–function correspondence need not be predictive during training, and post-hoc ablation severity must not be read as developmental necessity.

Companion work (context only). Companion work in preparation analyzes the *iterated* attention propagator with pseudospectral tools under mask-structure nulls; none of this paper’s

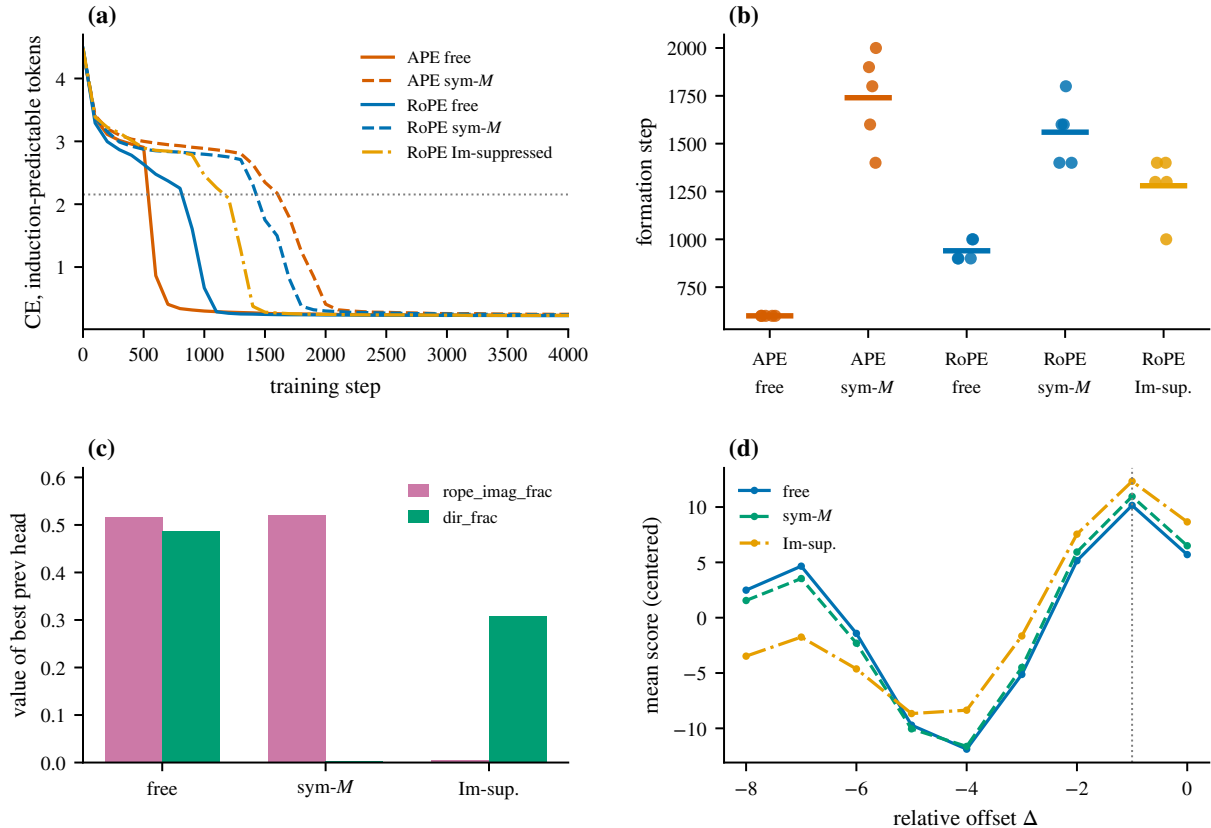


Figure 5: Constrained-training interventions. (a) induction-capability curves: every arm reaches the floor; constraints delay the drop. (b) formation times ($n=5$). (c) the dissociation: under sym- M the prev head keeps full phase content (`rope_imag_frac`) with a fully symmetric static M (`dir_frac` ≈ 0); under Im-suppression the reverse. (d) positional kernels: sym- M is indistinguishable from free (the kernel is carried by the untouched phase); Im-suppression reshapes the kernel but its peak stays at $\Delta=-1$ (reroute).

claims relies on it. We flag two of its directions as context: a division of labor consistent with our tool choice (eigenvalue-level summaries suffice for the static scoring form; resolvent-level tools are needed for the depth-iterated propagator), and a state-dependent character of induction heads that static weight fingerprints cannot capture — consistent with their content-like static profile in §4.

Limitations. (i) The RoPE evidence in §6–7 is correlational (shared-variance) over heads; §8 supplies causation but as a concentrated per-head effect (now on all three RoPE models). (ii) Three learned-absolute models are tested with a consistent strong-head profile but heterogeneous aggregate and moderate-band statistics, whose sources (training corpus; GPT-Neo’s alternating local attention) are unresolved; the ALiBi scheme is covered by a single model (BLOOM-1b1). (iii) Inference treats heads as units: heads share layers and training (layer-clustered design effects 3.6–6.9; we report clustered CIs), and Llama heads share K-projections within GQA groups of 4 (between-group variance 0.55–0.79) — group-level dependence is only partially resolved. (iv) Llama runs in bf16 (float64 metrics from bf16 weights are exact w.r.t. the model; the diagonal convention check matches to bf16 precision only). (v) Single-head ablations miss composition; the prev→induction wiring is verified by K-composition (§4) but full path patching is future work. (vi) QK biases lie outside M

and are held fixed in ablations; the prev-detector’s bulk-ordering reliability is unquantified. (vii) A non-Llama full-RoPE family (Qwen/Mistral) would broaden the third architecture point.

12 Conclusion

For the attention QK operator, the plain antisymmetric split describes head function architecture-generally; the complex-eigenvalue refinement earns its keep only under RoPE, where it tracks the rotational phase whose causal load head-level ablations establish. Tracking training shows this spectral signature is born at the random-matrix null, locks in with circuit formation, and is sculpted into today’s profiles after function arrives; constrained training shows it is a *default*, not a necessity — every spectral channel we blocked was rerouted around, at a significant and interpretable search cost. The non-Hermitian view of attention is neither uniformly profound nor uniformly decorative: *the positional scheme sets the default spectral algebra of attention’s solutions*, and we measure that claim statically, dynamically, and causally in the settings analyzed. Scaled constrained pretraining is its direct falsification path.

Reproducibility & pre-registration. Code in `src/`: `extract`, `decompose`, `metrics`, `observables`, `semantics`, `p4_rope`, `rope`, `p5_rope_ablation`, `p9_checkpoint_dynamics`, `p10_training_intervention`. Per-head tables: `results/cache/*_head_full.parquet`; checkpoint trajectories and training histories under `results/cache/`. The dynamics questions (Q1–Q3) and intervention predictions (P1–P4) were pre-registered in the project plan before data collection; falsified predictions (Q3, P2-strong, P3, P4-timing) are reported as such. The full artifact bundle — code, per-head tables, checkpoint trajectories, training histories, figure scripts, and the pre-registration documents — is released at <https://github.com/HengyuLi-Ozaki-lab/qk-spectral-fingerprint>; the repository’s version history stamps which analyses were specified before their data existed.

References

- [1] Federico Barbero, Alex Vitvitskyi, Christos Perivolaropoulos, Razvan Pascanu, and Petar Veličković. Round and round we go! what makes rotary positional encodings useful? In *International Conference on Learning Representations (ICLR)*, 2025. arXiv:2410.06205.
- [2] Alberto Bietti, Vivien Cabannes, Diane Bouchacourt, Hervé Jégou, and Léon Bottou. Birth of a transformer: A memory viewpoint. In *NeurIPS*, 2023. arXiv:2306.00802.
- [3] Po-Hao Chang. From embeddings to dyson series: Transformer mechanics as non-hermitian operator theory, 2026. arXiv:2603.11322.
- [4] Angelica Chen, Ravid Shwartz-Ziv, Kyunghyun Cho, Matthew L. Leavitt, and Naomi Saphra. Sudden drops in the loss: Syntax acquisition, phase transitions, and simplicity bias in mlms. In *ICLR*, 2024. arXiv:2309.07311.
- [5] Martin Courtois, Malte Ostendorff, Leonhard Hennig, and Georg Rehm. Symmetric dot-product attention for efficient training of BERT language models. In *Findings of ACL*, 2024. arXiv:2406.06366.

- [6] Nelson Elhage, Neel Nanda, Catherine Olsson, Tom Henighan, Nicholas Joseph, Ben Mann, et al. A mathematical framework for transformer circuits. *Transformer Circuits Thread*, 2021. <https://transformer-circuits.pub/2021/framework/index.html>.
- [7] Jesseba Fernando and Grigori Guitchounts. Dynamics of the transformer residual stream: Coupling spectral geometry to network topology, 2026. arXiv:2605.14258.
- [8] Huang et al. Dissecting multimodal in-context learning: Modality asymmetries and circuit dynamics in modern transformers, 2026. arXiv:2601.20796.
- [9] Shafayeth Jamil and Rehan Kapadia. The routing and filtering structure of attention, 2026. arXiv:2605.18826; concurrent work.
- [10] Nikita Kitaev, Lukasz Kaiser, and Anselm Levskaya. Reformer: The efficient transformer. In *ICLR*, 2020. arXiv:2001.04451.
- [11] Hengyu Li. Steering is cheaper than banning: Assistance-based selection of attention’s spectral solutions, 2026. Companion note; preprint.
- [12] Beren Millidge and Sid Black. The singular value decompositions of transformer weight matrices are highly interpretable. *AI Alignment Forum / Conjecture*, 2022. <https://www.alignmentforum.org/posts/mkbGjzxD8d8XqKHZA>.
- [13] Catherine Olsson, Nelson Elhage, Neel Nanda, Nicholas Joseph, et al. In-context learning and induction heads. *Transformer Circuits Thread*, 2022. arXiv:2209.11895.
- [14] Gautam Reddy. The mechanistic basis of data dependence and abrupt learning in an in-context classification task. In *ICLR*, 2024. arXiv:2312.03002.
- [15] Matteo Saponati, Pascal Sager, Pau Vilimelis Aceituno, Thilo Stadelmann, and Benjamin Grewe. The underlying structures of self-attention: symmetry, directionality, and emergent dynamics in transformer training. In *International Conference on Machine Learning (ICML)*, 2025. arXiv:2502.10927.
- [16] Aaditya K. Singh, Ted Moskowitz, Felix Hill, Stephanie C.Y. Chan, and Andrew M. Saxe. What needs to go right for an induction head? a mechanistic study of in-context learning circuits and their formation. In *ICML*, 2024. arXiv:2404.07129.
- [17] Jianlin Su, Yu Lu, Shengfeng Pan, Ahmed Murtadha, Bo Wen, and Yunfeng Liu. RoFormer: Enhanced transformer with rotary position embedding. *Neurocomputing*, 2024. arXiv:2104.09864 (2021).
- [18] Curt Tigges, Michael Hanna, Qinan Yu, and Stella Biderman. Llm circuit analyses are consistent across training and scale. In *NeurIPS*, 2024. arXiv:2407.10827.
- [19] Felipe Urrutia, Jorge Salas, Alexander Kozachinskiy, Cristian Buc Calderon, Hector Pasten, and Cristobal Rojas. Decoupling positional and symbolic attention behavior in transformers, 2025. arXiv:2511.11579.
- [20] Kevin Wang, Alexandre Variengien, Arthur Conmy, Buck Shlegeris, and Jacob Steinhardt. Interpretability in the wild: a circuit for indirect object identification in GPT-2 small. In *International Conference on Learning Representations (ICLR)*, 2023. arXiv:2211.00593.